Journal of *Marine Science and Engineering*

MDPI

Article

Improved Performance of Wave Energy Converters and Arrays for Wave-to-Onshore Power Grid Integration

Madelyn Veurink [1,*], David Wilson [2], Rush Robinett [3] and Wayne Weaver [3]

[1] Electrical and Computer Engineering, University of Michigan, Ann Arbor, MI 48109, USA
[2] Sandia National Labs, Albuquerque, NM 87123, USA; dwilso@sandia.gov
[3] Department of Mechanical and Aerospace Engineering, Michigan Technological University, Houghton, MI 49931, USA; rdrobine@mtu.edu (R.R.); wwweaver@mtu.edu (W.W.)
* Correspondence: mveurink@umich.edu

Abstract

This paper focuses on power grid integration of wave energy converter (WEC) arrays that minimize added energy storage for maximizing power capture as well as smoothing the oscillatory power inputs into the grid. In particular, a linear right circular cylinder WEC array that implements complex conjugate control is compared and contrasted to a nonlinear WEC array that implements an hourglass buoy shape while both are integrated into the grid utilizing phase control (i.e., relative spacing of the WEC array) on the input powers to the grid. The Hamiltonians of the two WEC systems are derived, enabling a direct comparison of real and reactive power, with reactive power reflecting the utilization of stored energy. The control systems are simulated in MATLAB/Simulink under both regular wave conditions and irregular seas generated from a Bretschneider spectrum. For the linear right circular cylinder buoy, the proportional-derivative complex conjugate controller requires an external energy storage device to supply reactive power, whereas the nonlinear hourglass buoy inherently provides reactive power through its geometric design. This study demonstrates that: (i) The unique geometry of the hourglass buoy reduces the required energy storage size for the nonlinear system while simultaneously increasing power output. (ii) Phase control of the hexagonal hourglass array further enhances real power capture. Together, these effects substantially decrease the size and demand on the individual buoys and grid integration energy storage requirements.

Keywords: wave energy converter; nonlinear control; complex conjugate control; energy storage systems

Academic Editors: Atilla Incecik and Decheng Wan

Received: 7 October 2025
Revised: 1 December 2025
Accepted: 2 January 2026
Published: 15 January 2026

1. Introduction

There is a significant abundance of untapped marine energy potential in the ocean worldwide. Marine energy technologies convert the energy of ocean waves, tides, and currents, as well as river currents, into electricity and other forms of usable energy. The marine energy resource potential in the United States is significant and geographically diverse, with a study commissioned by the U.S. Department of Energy estimating that the nation's annual marine energy potential is approximately 2300 TWh/year across the 50 states, or greater than 57 percent of U.S. electricity generation in 2019 [1]. However, the marine energy industry still faces hurdles to commercialization; high cost of development, manufacturing, reliability, maintenance, grid integration, and technological maturity [2]. Economically for marine energy technology to become practical many of these hurdles

need to be overcome. For ocean waves, one popular device, wave energy converters (WEC), needs significant improvements in power absorption and wave-to-wire efficiency [3,4], To supply appropriate power to the utility grid, WECs require energy storage capacity with supporting power electronic conversion. These components are essential for converting the oscillatory energy derived from ocean waves into a consistent reliable supply of generated power.

Research efforts are needed to focus on incorporating complimentary WEC energy storage systems to harmonize in balancing integrated supply and demand. In addition, detailed grid impact studies are required to assess the effects of large-scale wave energy deployment on grid stability. Advancing WEC designs [3,5,6] that deliver more consistent power are critical for efficient grid integration [7]. Generating electricity from the waves in the ocean requires the use of power-take-off (PTO) devices for each of the WEC buoys [8]. Large arrays of WEC farms can capture the initial power, however, how to phase and optimize this marine power to the shoreline utility power grid is still a large research topic. Minimizing the amount, size, and type of energy storage is still an open issue. An example, is given in [9] of a specific energy storage system coupled to the WEC that utilized super capacitors to provide constant power out. In comparison, others reviewed the upgrade of a fly-wheel energy storage system to a hydraulic system [10]. Energy storage is necessary for proper operation of these WECs but the large installation cost of these systems can negatively impact the LCOE. To maximize the power delivered to the utility grid, losses in the system must be minimized while power absorbed by the WECs must be maximized. In addition to maximizing the WEC power absorbed challenges associated with the irregular wave operating environment need to be overcome.

The wave environment in which a WEC operates can be represented as an irregular wave composed of multiple sinusoidal frequency components. Such irregular waves are often characterized using wave spectra, such as the Bretschneider Spectrum. The Bretschneider Spectrum is generated using the peak frequency and significant wave height of the ocean waves at a given time [11]. As ocean waves vary with the seasons and time of day, different spectra can be generated to represent different conditions at a given location [12]. Daily and seasonal variations in the wave spectrum make it challenging to maximize energy absorption by the WEC.

Several control strategies are given in the literature that are designed to maximize energy capture. One popular approach uses linear control to resonate the WEC with dominate frequencies in the wave spectra to increase power capture, see [6]. Most recently, the shape of the buoy can be altered, to produce inherent energy storage (reactive power) through nonlinear interactions with the wave force, see [13].

Exploring further, a linear complex conjugate controller can be utilized on a cylindrical buoy to resonate the WEC with the varying wave spectra for a given condition. Two requirements must be met for proper operation: (i) the buoy must resonate with the excitation frequency and (ii) the added damping of the controller and the damping of the WEC system itself must be impedance matched [14,15]. In real-time the magnitude and phase of each frequency component in the wave spectra requires an estimator [7]. This is realized using PD feedback control. The proportional gain of the feedback loop is determined by calculating the magnitudes of the individual frequencies in the wave spectra. To maximize the power absorption, the derivative gain of the feedback controller is set equal to the mechanical impedance of the buoy [3,16], also known as Proportional Derivative Complex Conjugate Control (PDC3), see [3].

The nonlinear buoy has been previously studied in [3,13] where a nonlinear WEC is developed by designing the buoy in the shape of an hourglass. By exploiting the nonlinear hydrodynamic force, increased energy capture and reactive power reduction was

achieved [5]. The reactive power needed to resonate the WEC with the wave spectrum it operates in is uniquely produced by the hourglass shape of the buoy. The need for large conventional energy storage systems (battery, flywheel, capacitor, etc.) to supply the required reactive power is reduced. The real power is extracted through a simplified rate feedback controller.

Power packet networks were first introduced as electricity-power-packets in [17] to integrate variable energy resources into a larger utility power grids. Arranging multiple linear controlled WECs into power packet network arrays improved system robustness while increasing the power delivered to the grid from each array [7]. In addition, this helped to reduce the required size of the energy storage system while minimizing power variation and lowering cost/complexity. By coupling these desirable features and new advancements [7] the wave-to-wire efficiencies were enhanced while also providing a more resilient connection to the onshore utility power grid [18]. This work builds on [13] to develop two hexagonal WEC arrays as part of a power packet network. The optimal phasing for the linear array was investigated in [7]. Phasing reduces the required size of the energy storage for each array while maximizing the power delivered to the onshore utility power grid. This work extends [13] to determine the optimal phasing for the new nonlinear hourglass WEC array. To further increase power delivered to the grid, the steepness angle, alpha, for each hourglass buoy was adjusted to increase its power absorption.

Combining this WEC array phase control with the unique hourglass shape WEC improves the quality of power delivered to the grid and reduces peak reactive power which minimizes additional energy storage equipment. In addition, by adjusting the steepness angle, alpha, for the hourglass buoy, per sea state, increases the real power capture. This nonlinear hourglass buoy WEC is compared to the state-of-the-art PDC3 right circular cylinder buoy WEC while maintaining equivalent volumes, with respect to; size, weight, and power (better known as SWaP [19]). The goal is to minimize size and weight while increasing power or improving power and energy density per each individual and collective set of arrays for any given WEC marine power farm. Evidence of this claim are described below for increased PTO and grid power with minimal required energy storage. This feasibility or proof-of-concept study is the key contribution for this paper and successfully demonstrated the enhanced SWaP characteristics for the hourglass WEC design and unique power packet network array implementation.

This paper focuses on enhancing the performance of WECs from wave capture to onshore grid integration. It addresses both real and reactive powers, with particular emphasis on minimizing energy storage requirements by reducing reactive power demand while simultaneously increasing energy capture through advanced nonlinear control techniques. In this study, the nonlinear WEC array produced 42.96% more PTO power and delivered 79.22% more power to the grid compared to the linear array. The nonlinear buoy also required 52.86% less maximum reactive power than the linear buoy. At the utility scale, such analyses are essential for assessing both feasibility and economic viability. This paper is presented in seven Sections. In Section 2 models for both the right circular cylinder and nonlinear hourglass buoys are developed. In Section 3 the control designs are developed for both buoys. Section 4 describes the mechanical and electrical drive-train models. Section 5 introduces the wave spectrum inputs utilized for validation. Section 6 presents the numerical simulation results. The final Section 7 presents the concluding remarks.

2. Dynamic Buoy Models and Array Interaction

In this section, the dynamic buoy models are developed along with how the buoy arrays interact, respectively.

2.1. Right Circular Cylinder

The linear right circular cylinder buoy comparison being made in this study can be modeled as a mass-spring-damper (MSD) system. The equation of motion for a linear buoy in an array is

$$(m + m_a)\ddot{x} + b\dot{x} + k_{hs}x = f_e + f_u. \quad (1)$$

The mass of the buoys is described using the constant m and the added mass as m_a. The radiation damping of the linear buoy is b, the hydrostatic force constant of the buoys is k_{hs}, and f_e and f_u are the excitation and control forces acting on each of the buoys in the array. The excitation force on the right circular cylinder buoys is calculated as [13]

$$f_e = \rho g \pi r^2 \eta \quad (2)$$

where ρ is the density of water, g is the gravitational constant, η is wave elevation term, and r is the radius of the buoy. The control force on the right circular cylinder buoy is implemented as

$$f_u = (\omega^2 m_{RCC} - k_{RCC})x - b_{RCC}\dot{x}. \quad (3)$$

The hydrostatic force on the right circular cylinder buoy is generated due to the submerged volume of the buoy. It is calculated using the area of the buoy submerged in the water plane as in [20]. The hydrostatic spring constant is denoted by k_{hs} and is given by

$$k_{hs} = \rho g A_{wp} \quad (4)$$

where A_{wp} is the cross-sectional area of the buoy submerged in the water.

The added mass and the damping of the buoy were calculated using the BEM software, version 3.0. Nemoh [21]. The dimensions of the right circular cylinder buoy used in this study are shown in Table 1, and additional paramter information can be found in Appendix A.

Table 1. Buoy parameters.

Type	Radius (m)	Height (m)	Alpha (Deg)
right circular cylinder	0.41	0.50	–
hourglass	1.73/2	0.4483	75

The radius and height of the right circular cylinder buoy were used to calculate the volume of the buoy as

$$V_{RCC} = \pi r^2 h. \quad (5)$$

The mesh file created by Nemoh [21] to determine the added mass and radiation damping of the right circular cylinder buoy is shown in Figure 1.

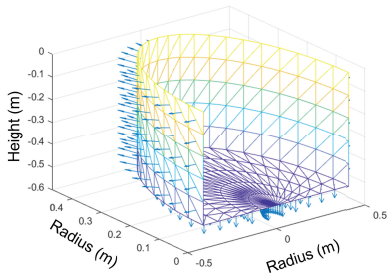

Figure 1. Right circular cylinder Buoy mesh file utilized in Nemoh BEM software [21].

The calculated added mass and radiation damping from Nemoh [21] for the right circular cylinder buoy are shown in Figure 2.

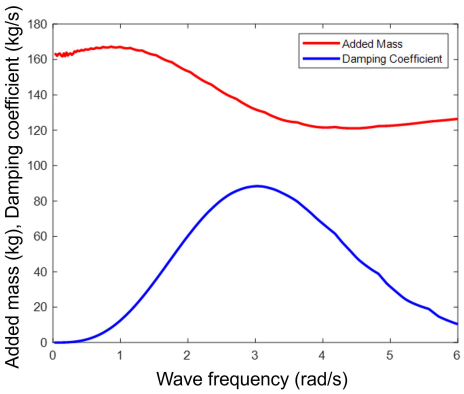

Figure 2. Added mass and damping coefficient for the right circular cylinder buoy calculated using Nemoh [21].

2.2. Hourglass

The nonlinear hourglass buoy modeled in this study was previously derived in [6]. The equation of motion for the hourglass buoy in an array is

$$m_{HG}\ddot{x} = -b_{HG}\dot{x} - m_{HG}g + \rho g V_{sub} + f_u. \tag{6}$$

The mass of each hourglass buoy is denoted by the constant m_{HG}. The radiation damping of each nonlinear buoy is represented by the constant b_{HG}, and the hydrostatic force keeping the buoy in the water is given by $m_{HG}g + \rho g V_{sub}$. V_{sub} in the equation of motion is replaced with

$$V_{sub} = V_{cone} + \pi\hat{\alpha}^2\left[\frac{1}{3}\eta^3 - x\eta^2 + x^2\eta - \frac{1}{3}x^3\right] \tag{7}$$

where α is the angle of the hourglass buoy, and η is the wave height. The value of α is a design parameter that may be varied as shown in Figure 3.

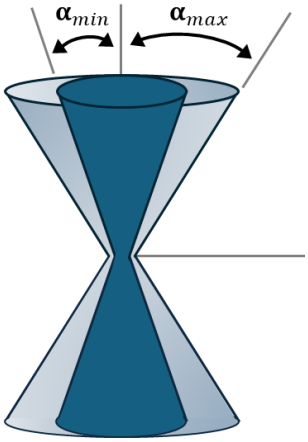

Figure 3. Hourglass buoy shape with α, defined as the steepness angle, showing α_{max} and α_{min}. The dark blue hourglass represent the buoy with the minimum steepness angle and the light blue represents the buoy with the maximum α.

The volumes of each of the hourglass buoy cones are calculated as

$$V_{cone} = \frac{1}{3}\pi r^2 h = \frac{1}{3}\pi \hat{\alpha}^2 h^3. \tag{8}$$

The volume of the cone is simplified by calculating the radius of the cone based on the height and angle of the cone as

$$r = h\tan(\alpha) \approx h\hat{\alpha}. \tag{9}$$

Substituting ((7)–(9)) into (6) results in the full equation of motion for the nonlinear buoys as

$$m_{HG}\ddot{x} + b_{HG}\dot{x} + \rho g\pi\hat{\alpha}^2\left[\frac{1}{3}x^3 - \eta x^2 + \eta^2 x\right]$$

$$= \frac{\rho g\pi\hat{\alpha}^2}{3}\eta^3 + F_u. \tag{10}$$

The unique shape of the nonlinear buoy generates a hydrostatic force on the buoy.

Note that for both buoys, the incident waves at the deployment sites of the right circular cylinder and hourglass WECs exert dynamic forces on each buoy within their respective arrays, and it is assumed that no hydrodynamic interaction occurs between buoys [16,22]. In Babarit [23] showed for a two-body array of heaving or surging WECs aligned with the direction of the incoming waves with large separation between buoys then the radiation is negligible. The energy absorption due to wave interaction effects decreases asymptotically with the square root of the separating distance. Accounts for the effects of radiation at closer distances is also discussed in [24]. The irregular sea states that the buoys are operating in can be described by the summation of the many different individual frequency components within the wave spectrum as

$$f_e = \sum_{n=1}^{N} A_n sin(w_n t + \phi_n) \tag{11}$$

where A_n, ω_n, and ϕ_n are the amplitude, frequency, and phase of each individual frequency component in the wave spectrum.

2.3. Arrays

The right circular cylinder and hourglass buoys were arranged in groups of six to form arrays. The buoys are arranged in arrays to reduce implementation costs by sharing standard components, including the energy storage system, DC bus, undersea cable, and shore-side grid inverter. The right circular cylinder array is formed by six right circular cylinder buoys connected in parallel to a shared dc bus and energy storage system. The hourglass array is formed by six hourglass buoys connected in parallel to a shared dc bus and energy storage system. Each array is modeled with a separate line to shore to study the power delivered to the grid from the two arrays. In practice, right circular cylinder and nonlinear arrays could share undersea cables connecting their DC buses to shore, further reducing costs. The right circular cylinder and hourglass buoy array formations with respect to the shore are shown in Figure 4.

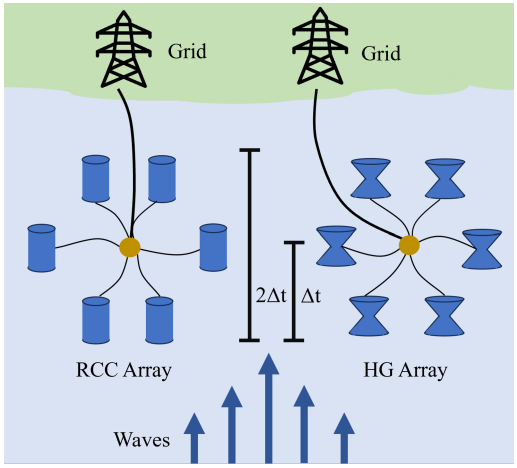

Figure 4. Formation of the right circular cylinder and hourglass arrays in the water with respect to the onshore utility power grid and incoming wave force.

3. Control Law Designs with Real and Reactive Power Terms

The control laws for each buoy are developed in each subsection. The first subsection designs a PDC3 system for the linear right circular cylinder buoy. The next subsection designs a simple rate feedback controller for the hourglass buoy, where the inherent energy storage is implicitly part of the nonlinear cubic spring effect see (10), due to the hourglass buoy and wave interactions. The next subsection introduces the power packet network phase control between buoys for each of the linear and nonlinear buoy arrays. The final subsection, defines the real and reactive power terms for each linear and nonlinear buoy arrays, respectively.

3.1. PDC3 Design

The controller for the right circular cylinder WEC array is based off of the previous work done in [7]. The position and velocity of the WEC are fed back to the controller and are decomposed into their individual cosine and sine components. The position is decomposed as

$$\hat{x}(t) = a_0 + \sum_{n=1}^{N} [a_n cos(n\omega t) + b_n sin(n\omega t)] \tag{12}$$

where a_0 is the average value of $x(t)$, and a_n and b_n correspond to the amplitudes of the sine and cosine components of one frequency in the excitation force. The velocity is decomposed similarly as

$$\hat{v}(t) = c_0 + \sum_{n=1}^{N} [c_n cos(n\omega t) + d_n sin(n\omega t)]. \tag{13}$$

To maximize energy extraction, each WEC is controlled to resonate with the peak frequency of the wave spectrum. This impedance-matching control strategy has been explored in [13,15]. Achieving resonance with the dominant wave frequencies requires calculating the amplitudes of the individual spectral components and designing a controller for each peak frequency. Using a Sequential Least Squares Estimator (SLSE), the amplitudes of the sine and cosine components of each frequency can be determined as

$$x_n = [a_1, b_1, ..., a_n, b_n]^T = x_{n-1} + PA^T(Y - Ax_{n-1}) \tag{14}$$

where the weighting matrix is P, A is the matrix containing the amplitudes for the sine and cosine components of the frequency, Y is the measured values to be estimated, and x_{n-1} is the previous sine and cosine amplitude estimates for an individual frequency [25].

Using the individual frequency component amplitude values, calculated from the SLSE, a linear PDC3 controller can be implemented on the WEC array [7]. To enable PDC3 on the buoy, the irregular wave excitation force must be divided into its individual frequency components. For each of the individual frequency components, a proportional derivative controller may be used to resonate the buoy with the respective frequency and maximize the power absorption. Resonating the buoy with the individual frequency fulfills the first requirement of complex conjugate control, and impedance matching fulfills the second requirement [14]. Each of the individual frequency PD control channels will then be summed together to create the full multi-frequency control force for the right circular cylinder buoy. The PDC3 controller process is shown in Figure 5.

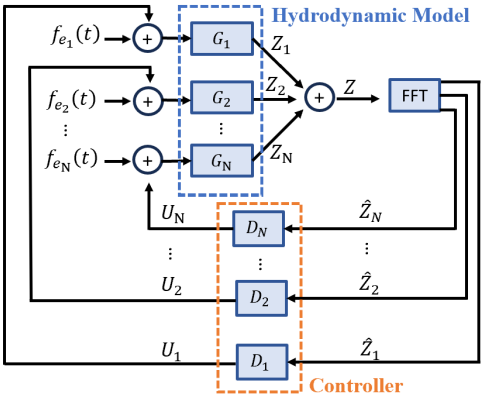

Figure 5. Block diagram of WEC system with PDC3.The transfer functions G_N represent the systems hydrodynamics and D_N represent the controllers for each frequency channel.

To resonate the right circular cylinder WEC with the wave force, the proportional gain of PDC3 for each frequency is calculated as

$$k_{p,i} = \omega_i^2 m - k_{hs}. \tag{15}$$

The derivative gain in the PD controller is designed to maximize the power absorbed by the buoy. This is accomplished through impedance matching by equating the real part of the control impedance to the real part of the mechanical impedance. The derivative gain is calculated as

$$k_{d,i} = b. \tag{16}$$

The complete irregular wave control force for the right circular cylinder WEC is created by summing together each of the individual frequency PD control channels to create an irregular wave control force.

3.2. Nonlinear Control Design

The unique shape of the nonlinear buoy physically interacts with the waves that generates a hydrostatic force which is explicitly identified as $\rho g \pi \hat{a}^2 \frac{1}{3} x^3$, from the analytic model (10). This is a cubic spring like restoring term, with the same effect as an energy storage system leading to reactive power. It is important to point out that reactive forces do no work over the cycle, but provide necessary oscillatory exchange of energy to generate real power derived from the rate feedback controller. The rate feedback control force applied to the nonlinear buoy is determined from

$$F_u = -R_{opt} \dot{x} \tag{17}$$

where R_{opt} is the feedback constant which can be optimally selected as in [13]. Since the hourglass buoy shape itself provides the required reactive power, the control law reduces to rate feedback, eliminating the need for additional reactive power from external devices. It is observed that the rate feedback gain can be increased to just under overtopping while the coordinated adjustment of the steepness angle, per varying sea state wave, will help to produce the maximum real power potential from the hourglass buoy design.

3.3. Buoy Phasing Control

The hourglass and right circular cylinder controllers tune each buoy to resonate with the incoming wave force, driving the device at the dominant wave frequency. At resonance, the device velocity is in phase with the excitation force, so the power factor is one. If the arrays are operating in a sinusoidal regular wave sea state, each WEC will output power as

$$p_i(t) = cos^2(\omega_n t) = \frac{1}{2}(cos(2\omega_n t) + 1). \tag{18}$$

Shifting the buoys within a WEC array introduces a phase shift, ϕ, between the electrical signals of each WEC. When the electrical signals from each WEC in the array are shifted at phase ϕ and the sinusoidal wave is at a frequency of ω_n, the output power from each of the WECs in the array becomes

$$p_i(t) = \frac{1}{2}(cos(2\omega_n t - 2(i-1)\phi) + 1). \tag{19}$$

The sum of all the powers of N WECs in an array then becomes

$$\begin{aligned} P_{array} &= \sum_{i=1}^{N} p_i(t) \\ &= \frac{1}{2}(csc(\phi)sin(N\phi)cos(2\omega_n t + \phi(1-N))) + N). \end{aligned} \tag{20}$$

The sum of the power from the array will be constant when

$$csc(\phi)sin(N\phi) = 0. \tag{21}$$

Which happens when the buoys are phase shifted at the conditions

$$\phi \in \left\{ \frac{\pi}{N}, \frac{2\pi}{N} \right\}. \tag{22}$$

When the six WECs in the right circular cylinder and hourglass arrays are grouped into three pairs, the two devices in each pair operate in unison, effectively behaving as a single, larger WEC. The array can produce a constant total power output when the positions of the WECs in the water create a "phasing" of $\pi/3$ rad $= 60^\circ$ or $2\pi/3$ rad $= 120^\circ$ apart in time [7].

A constant power output from each of the right circular cylinder and hourglass arrays has many advantages. These advantages include: reducing the need for energy storage on the electrical bus, a reduction in the voltage ripple on the electrical bus, and an increase in power delivered to the grid due to fewer losses through the entire system. Due to the irregular wave conditions and multiple wave frequencies, it's unlikely to achieve a perfect phase shift that results in constant power output and a power factor of one. Instead, there will be a time shift between the buoys that leads to small variations in the total power from the array.

3.4. Real and Reactive Power Terms

The real and reactive powers used by the controllers in the right circular cylinder and hourglass buoys can be calculated using the equations of motion and the Hamiltonian's of the systems. The real power absorbed by the control system for the right circular cylinder buoy can be determined by multiplying the control force in (3) by the velocity $\dot{x}$. The real power portion from (3) then becomes

$$P_{RCC} = -b\dot{x}^2 \tag{23}$$

and the reactive power can be calculated as

$$Q_{RCC} = (\omega^2 m - k_{hs})x\dot{x}. \tag{24}$$

The real power captured by the controller on the nonlinear hourglass buoy can be determined by multiplying (17) once again by the velocity, $\dot{x}$. The real power absorbed by the hourglass buoy controller is

$$P_{HG} = -R_{opt}\dot{x}^2. \tag{25}$$

The reactive power for the nonlinear buoy can be calculated by taking the derivative of the Hamiltonian of (10). The Hamiltonian is defined as

$$H_{HG} = \frac{1}{2}m_{HG}(\dot{x})^2 + \frac{1}{12}k_{HG}(\alpha)x^4 \tag{26}$$

and the derivative of the Hamiltonian of the hourglass buoy is

$$\dot{H_{HG}} = m_{HG}\ddot{x}\dot{x} + \frac{1}{3}k_{HG}(\alpha)x^3\dot{x} \tag{27}$$

where $k_{HG}(\alpha)$ is $\pi\rho g\hat{\alpha}^2$. Using the derivative of the Hamiltonian for the hourglass WEC the reactive power (provided by the nonlinear hourglass geometry) used by the controller is

$$Q_{HG} = \frac{1}{3}k_{HG}(\alpha)x^3\dot{x}. \tag{28}$$

The primary distinction in the real and reactive powers of the right circular cylinder and the hourglass buoys lies in the origin of the reactive power. Unlike the right circular cylinder buoy, which relies on a large energy storage system, the hourglass buoy generates reactive power through its unique buoy shape. This inherent generation of reactive power from the hourglass buoy's shape allows for a smaller energy storage in the associated control system. This leads to real power from rate feedback control given in (17).

4. Mechanical and Electrical Drive-Train

Generating electricity from the waves in the ocean utilizes a power-take-off (PTO) device for each of the WEC buoys [8]. Direct drive PTOs, such as a rack-and pinion, generate a rotational velocity from the heaving vertical motion of the buoy. The power generated by the buoy's electric machine is converted through power electronics into dc power and sent to the dc bus. The dc bus connects to the onshore utility grid via an undersea cable and inverter, enabling power transfer to the grid [9].

For this study, a rack-and-pinion PTO is selected to convert the vertical heave velocity of the buoys to rotational velocity. The rotational velocity turns an electric machine for both hourglass and right circular cylinder buoy configurations (see Figure 6).

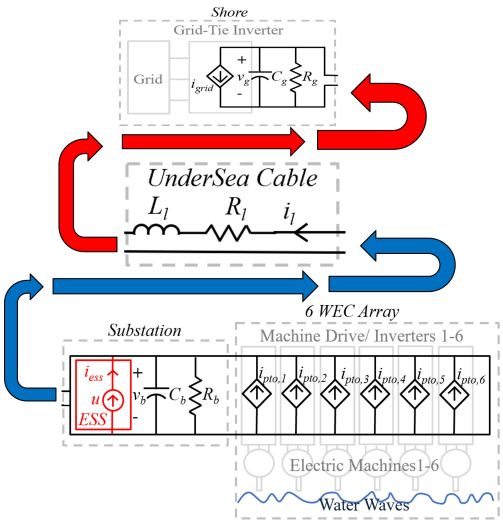

Figure 6. Wave to utility power grid electrical schematic.

The heaving linear motion of each of the buoys is converted to a rotation velocity by the PTO through a gear radius as

$$v_i = \dot{x}_i = r w_{m,i} \tag{29}$$

where v_i is the linear velocity of each of the hourglass and right circular cylinder buoys, $\dot{x}_i$ is the velocity of each buoy, r is the machine gear radius of the permanent magnet DC (PMDC) machine, and $w_{m,i}$ is the rotational velocity. The rotational velocity generated by the rack-and-pinion gear system is used to turn the electric machine on each of the right circular cylinder and hourglass buoys and generate power.

The individual arrays of six nonlinear hourglass WECs and six right circular cylinder linear WECs have a PMDC electrical machine on each of the buoys. The six electric machines in each array are then connected to an electrical energy storage bus. The energy from the bus is then transported via the undersea cable to the onshore electrical grid. The PMDC machine on each of the right circular cylinder and hourglass buoys can be modeled as

$$\frac{di_{a,i}}{dt} = \frac{1}{L_a}(v_{a,i} - i_{a,i}R_a - \frac{K_m v_i}{r}). \tag{30}$$

The power produced by each of the machines in the right circular cylinder and hourglass arrays sends power to the electrical energy storage bus as

$$i_{pto,i} = \frac{P_{pto,i}}{v_b} = \frac{v_{a,i} i_{a,i}}{v_b}. \tag{31}$$

The electric machines on the right circular cylinder and hourglass buoys are connected to their individual electrical buses in parallel. The sum of the currents into the separate dc busses from the six buoy arrays can be calculated as

$$i_{ptosum} = \sum_{i=1}^{N} i_{pto,i}. \tag{32}$$

Each of the underwater dc electrical buses is modelled as a parallel combination of a resistor, a capacitor, and an ideal energy storage system. Each of the substations are connected, individually, to the onshore electrical grid via an undersea cable that is 1 km long. The connections to the onshore electrical grid are modeled by a parallel combination

of a resistor, a capacitor, and a current source to represent the power being injected into the grid by each of the WEC arrays. Each of the substations can be modeled as

$$\dot{v_b} = \frac{1}{C_b}(i_{ptosum} - \frac{v_b}{R_b} - u - i_L) \tag{33}$$

where u is the ideal current injected into each of the individual substations from the energy storage systems as

$$u = \frac{v_{sc} - v_b}{R_{ESR}}. \tag{34}$$

The 1 km long undersea cables and grid connections can be modeled as

$$\frac{di_L}{dt} = \frac{1}{L_L}(v_b - i_L R_L - v_g) \tag{35}$$

$$\frac{dv_g}{dt} = \frac{1}{C_g}(i_L - i_{grid} - \frac{v_g}{R_g}). \tag{36}$$

5. Bretschneider Wave Spectrum

The irregular wave sea states that the right circular cylinder and hourglass WECs are operating in can be described using a wave spectrum, such as a Bretschneider spectrum. The Bretschneider spectrum is calculated as a function of the peak period and the significant wave height of the sea state during a given period in time [26]. The Bretschneider spectrum is calculated as

$$S(w) = \frac{5}{16}\frac{w_m^4}{w^5}H_{m0_{1/3}}^2 e^{-5\frac{w_m^4}{w^5}} \tag{37}$$

where w_m is the peak frequency of the waves, and H_{m0} is the significant wave height of a given sea state. The Bretschneider spectrum for this study was developed with the Wave Analysis for Fatigue Oceanography (WAFO) toolbox for MATLAB 2022a [27]. The `Bretschneider` function within the WAFO toolbox creates the desired wave spectrum based on user-entered parameters for the significant wave height, peak period, decay factor, and spectrum width. The values for the significant wave height and peak frequency are shown in Table 2. The WAFO `Bretschneider` function was used to create a frequency spectrum, which was then converted to a time domain spectrum using the WAFO `spec2dat` function. The time domain wave height is shown in Figure 7. The time domain wave data was then input into the right circular cylinder and hourglass buoy models and was used to calculate the excitation force acting on each of the buoys in the two arrays. The time domain wave height generated with the `spec2dat` function was converted to the frequency domain using MATLAB's built-in `FFT function`. The frequency domain for the wave height is shown in Figure 8. The four highest amplitude frequencies in the wave height frequency spectrum were then chosen to tune four PDC3 control channels on the right circular cylinder WEC. The four chosen frequencies for the control channels are shown in Table 3.

Table 2. Peak Period and Significant Wave Height in Bretschneider Spectrum.

Parameter	Value
Peak Period	12 [s]
Sig. Wave Height	1.2 [m]

Table 3. Frequencies in the wave height used to tune four PDC3 controller channels on the right circular cylinder buoys.

Channel	Frequency (Hz)
1	0.085
2	0.0915
3	0.074
4	0.0955

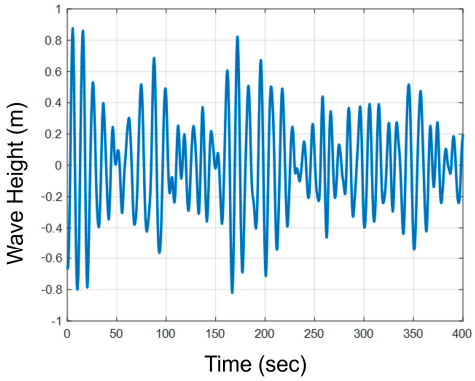

Figure 7. The time domain wave height generated from the Bretschneider spectrum. The wave height and frequency were collected from [28].

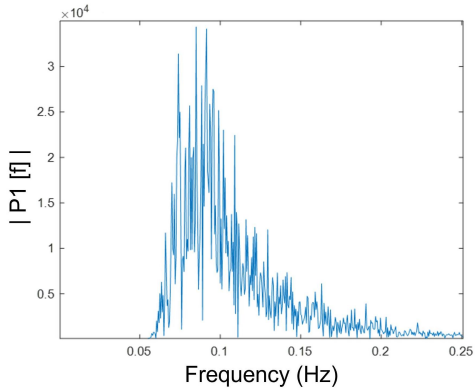

Figure 8. The frequency spectrum of the Bretschneider wave height generated using the WAFO toolbox. (single-sided amplitude spectrum of wave force). The wave height and frequency were collected from [28].

6. Results

Minimizing the variation in both real and reactive power is critical for reducing the size of the energy storage in the WEC systems. Large fluctuations in power require the energy storage to absorb or supply energy to maintain a stable grid connection, increasing both the required capacity and cost. By controlling each WEC to resonate with the dominant wave frequencies, the real power output is maximized and nearly sinusoidal, while the reactive power needed to maintain resonance is supplied by the buoy dynamics (as in the hourglass buoy) or through control (as in right circular cylinder). When the fluctuations in real and reactive power are small, the energy storage only needs to compensate for minor deviations, significantly reducing its required capacity. Furthermore, arranging WECs into power packet networks introduces additional smoothing of the aggregate power by phase-shifting the individual WEC outputs, further minimizing instantaneous power variation. Consequently, both the peak and average demands on the energy storage are reduced, lowering cost and improving overall wave-to-wire efficiency.

The right circular cylinder and hourglass buoy models were first simulated using a regular wave. The individual buoys were tested with this wave input to verify proper operation of the controllers and the energy torage systems. They were then tested in arrays of three buoys and six buoys. The regular wave had a height of 0.5 m and a period of 10 s.

A single right circular cylinder and hourglass buoy, each with equal volumes, was simulated in a regular wave state, and their controllers' real and reactive power were compared. The real and reactive powers used by the control systems for the linear right circular cylinder buoy and the nonlinear hourglass buoy are shown in Figures 9 and 10. The average real power generated by each of these buoys is shown in Table 4.

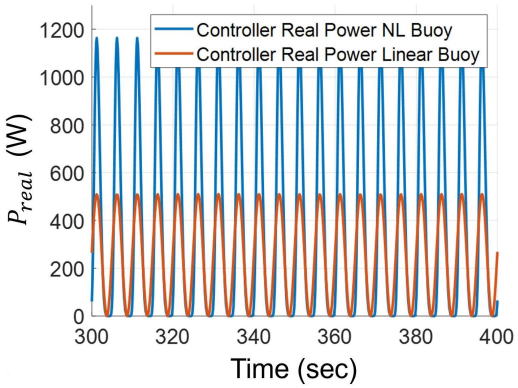

Figure 9. Real power captured by the controllers in the linear right circular cylinder and nonlinear hourglass buoys for a single frequency sinusoidal wave environment.

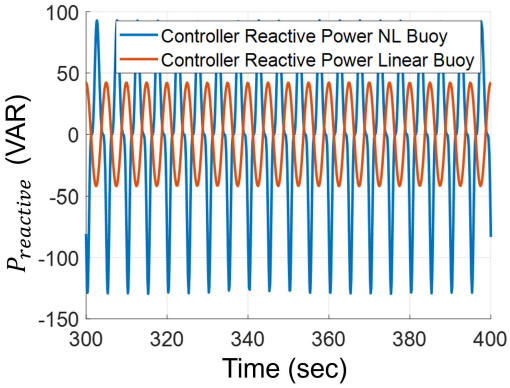

Figure 10. Reactive power used by the controllers in the linear right circular cylinder and nonlinear hourglass buoys for a single frequency sinusoidal wave environment.

Table 4. PTO power generated by the right circular cylinder and hourglass buoys in a sinusoidal wave environment.

Buoy	PTO Power [W]
linear right circular cylinder	245
nonlinear hourglass	373

Figures 9 and 10 show that for the individual buoys operating in a regular wave environment, the nonlinear hourglass buoy requires a larger energy storage for grid connection than the linear buoy due to the larger variation in the real and reactive powers of the controller. However, the nonlinear hourglass buoy does generate more power than the linear right circular cylinder buoy in the simple sinusoidal wave environment. The study in the regular wave environment was then extended by adding two right circular cylinder

and hourglass buoys to create two arrays of WECs. The arrays were first simulated with no time shift between the buoys, such that the incoming wave exerted a force on the buoys at the same time. The buoys were then shifted to a 60° phase shift with respect to the period of the wave height, and the variation in the real and reactive power used by the control systems was recorded. Figures 11 and 12 show the real and reactive power, respectively, for the three WEC arrays of linear and nonlinear buoys without a phase shift. Figures 13 and 14 illustrate the real and reactive power used by the controllers for both linear and nonlinear buoys, with a 60° phase shift between buoys in the arrays. The linear buoy maintains a nearly constant power output, while the nonlinear buoy exhibits reduced power variation.

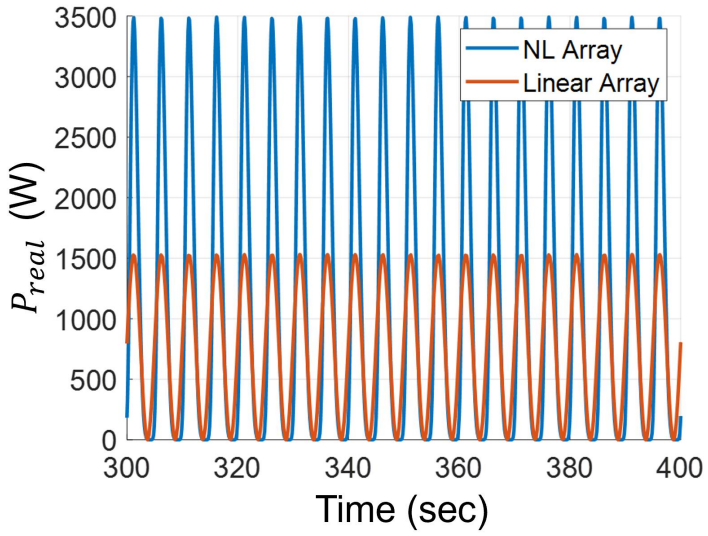

Figure 11. Real power captured by the controllers in the linear right circular cylinder and nonlinear hourglass three buoy arrays for a single frequency sinusoidal wave environment with no phase shift between the buoys.

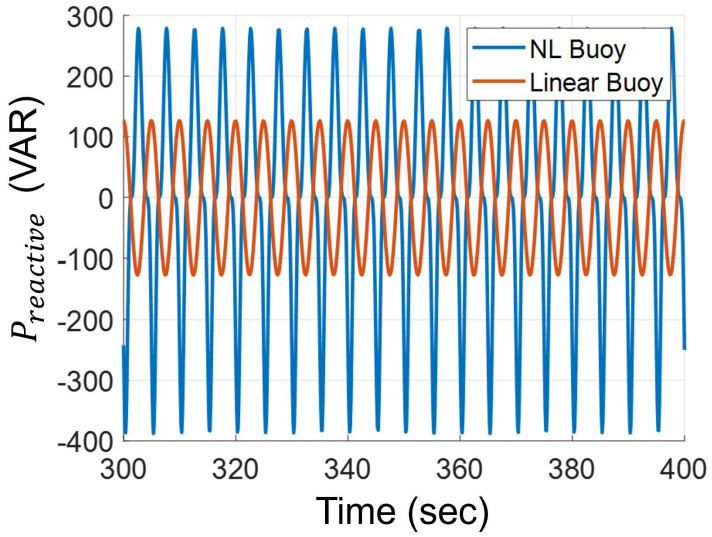

Figure 12. Reactive power used by the controllers in the linear right circular cylinder and nonlinear hourglass three buoy arrays for a single frequency sinusoidal wave environment with no phase shift between the buoys.

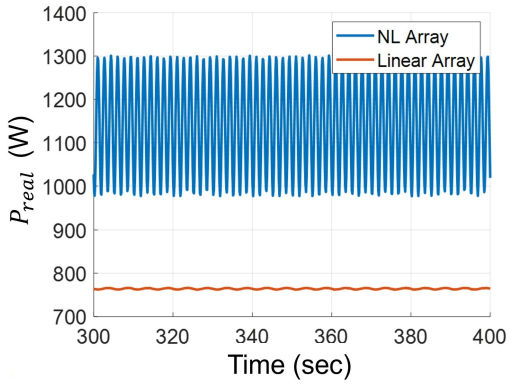

Figure 13. Real power captured by the controllers in the linear right circular cylinder and nonlinear hourglass three buoy arrays for a single frequency sinusoidal wave environment with a 60° phase shift between the buoys.

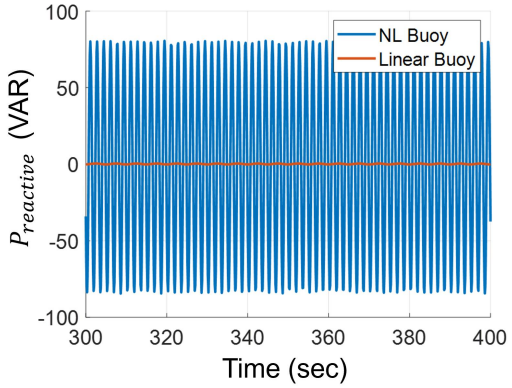

Figure 14. Reactive power used by the controllers in the linear right circular cylinder and nonlinear hourglass three buoy arrays for a single frequency sinusoidal wave environment with a 60° phase shift between the buoys.

The linear right circular cylinder and nonlinear hourglass buoy arrays were then simulated using excitation force and wave height data generated from the Bretschneider spectrum, as described in Section 5. The linear right circular cylinder and nonlinear hourglass buoy arrays were first simulated in the Bretschneider sea-state with no time shift between the buoys. The real and reactive powers used by the control systems for the arrays are shown in Figures 15 and 16, respectively.

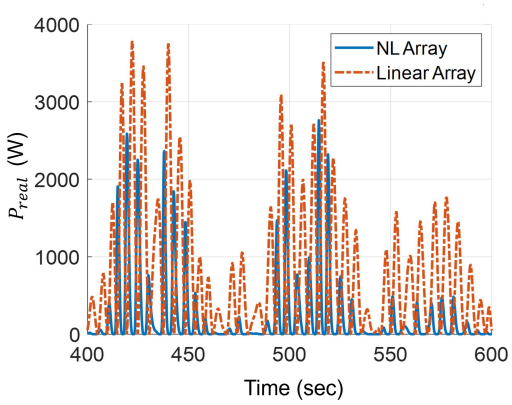

Figure 15. Real power captured by the controllers in the linear right circular cylinder and nonlinear hourglass three buoy arrays in a Bretschneider wave environment with no phase shift between the buoys.

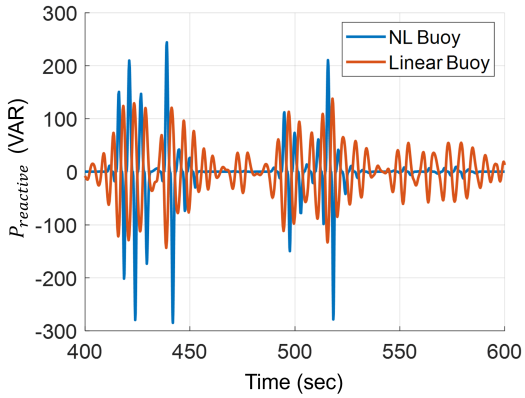

Figure 16. Reactive power used by the controllers in the linear right circular cylinder and nonlinear hourglass three buoy arrays in a Bretschneider wave environment with no phase shift between the buoys.

The three WECs in each of the linear and nonlinear arrays were then shifted to a 60° phase shift with respect to the peak frequency in the Bretschneider spectrum. This corresponded to a shift of 3.92 seconds between each of the buoys. The real and reactive powers required by the control systems on the linear right circular cylinder and nonlinear hourglass buoys are shown in Figures 17 and 18, respectively.

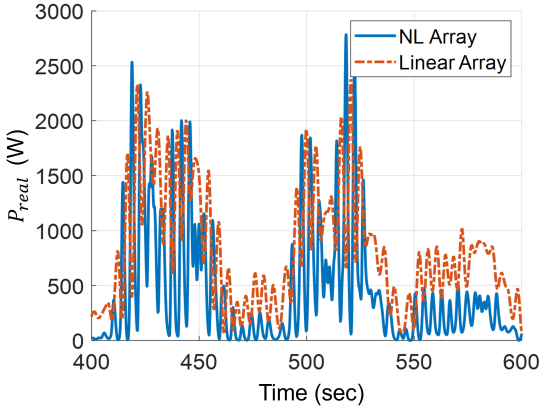

Figure 17. Real power captured by the controllers in the linear right circular cylinder and nonlinear hourglass three buoy arrays in a Bretschneider wave environment with a 60° phase shift between the buoys.

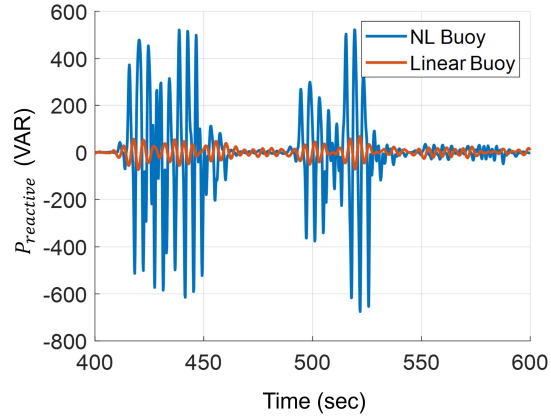

Figure 18. Reactive power used by the controllers in the linear right circular cylinder and nonlinear hourglass three buoy arrays in a Bretschneider wave environment with a 60° phase shift between the buoys.

From Figures 17 and 18 it can be observed that while a 60° phase shift reduces real power variations for the linear right circular cylinder buoy, it does not have the same effect on the nonlinear hourglass buoy, which still exhibits large variations in both real and reactive power. The nonlinear buoy was then adjusted to identify the time shift between buoys that minimizes real power variation and peak reactive power, thereby reducing the required size of the energy storage for the nonlinear array. The variations in the real and reactive powers for the nonlinear hourglass buoy control system for varying time shifts are shown in Table 5. The results were simulated on an array of six hourglass buoys divided into two groups of three, effectively treating each group as a single large buoy. This configuration was simulated eleven times, with one simulation including an additional one-second time offset for the second group. The additional one-second offset was tested to assess whether a slight de-synchronization could further smooth the array's power output.

Table 5. Variations in the Control System Powers for the nonlinear hourglass Array for Different Time Shifts Between the Buoys. The buoys were shifted over 11 different experiments.

Exp.#	Δt Group1 [s]	Δt Group2 [s]	ΔP_{real} [W]	ΔP_{react} [VAR]
1	0	0	8510	3098
2	1	1	1423	598
3	2	2	1421	586
4	3	3	1419	591
5	3.33	3.33	817	778
6	3.33	3.33 + 1	259	239
7	4	4	1422	588
8	5	5	8500	3088
9	6	6	1424	588
10	6.67	6.67	832	773
11	7	7	1417	590

The hourglass buoys were divided into two groups of three, with a 60° phase shift between the buoys and an additional one-second delay between the groups. This arrangement was selected to reduce peak reactive power generation while increasing real power output. These results were then applied to the linear right circular cylinder and nonlinear hourglass six WEC arrays operating in a Bretschneider wave environment. The real and reactive powers for the linear right circular cylinder and nonlinear hourglass six WEC arrays are shown in Figures 19 and 20, respectively.

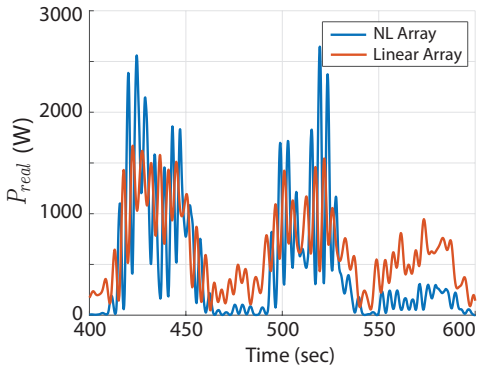

Figure 19. Real power captured by the controllers in the linear right circular cylinder and nonlinear hourglass six buoy arrays in a Bretschneider wave environment in Experiment 6 in Table 5.

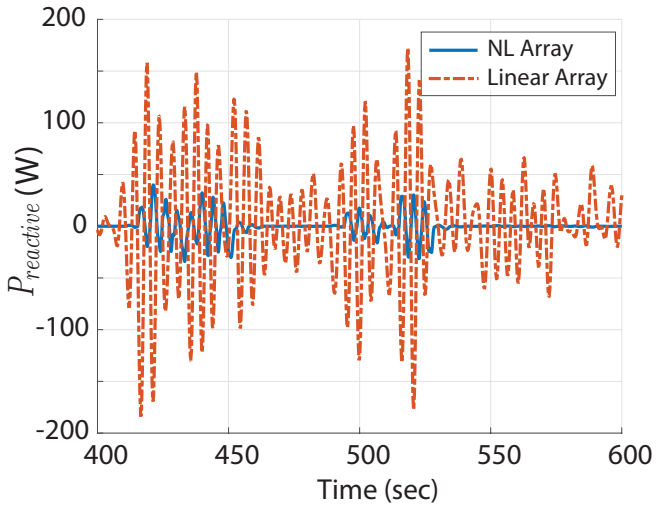

Figure 20. Reactive power used by the controllers in the linear right circular cylinder and nonlinear hourglass six buoy arrays in a Bretschneider wave environment with a 60° phase shift between the buoys with additional offset between the second group.

Figures 19 and 20 show that the control systems for the right circular cylinder and hourglass arrays use a similar amount of real power, with the hourglass array using less power during some periods. However, the reactive power requirements of the hourglass controller are much lower than those of the right circular cylinder WEC array. Additionally, the power delivered to the onshore grid from the nonlinear hourglass array is more than that of the linear right circular cylinder array. The PTO power generated by both the linear right circular cylinder array and the nonlinear hourglass array, along with the corresponding power delivered to the onshore grid, are shown in Figures 21 and 22, respectively. The grid power is computed as the sum of the array's PTO outputs after accounting for energy storage losses and cable transmission losses. While both arrays generate comparable levels of PTO power, the nonlinear hourglass array delivers noticeably more power to the grid. This improvement is due to the unique hourglass geometry, which supplies part of the reactive power, thereby reducing the burden on the energy storage and minimizing conversion losses.

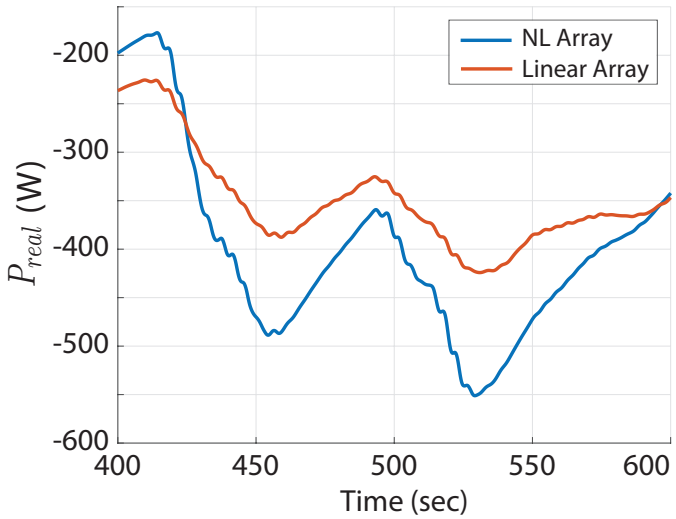

Figure 21. Power generated by the PTO on the linear right circular cylinder and nonlinear hourglass six WEC arrays with a 60° phase shift between the buoys with additional offset in the second group of buoys.

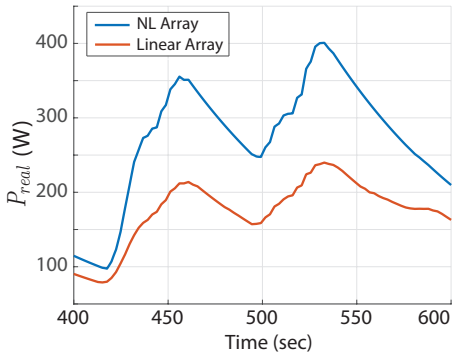

Figure 22. Power delivered to the grid by the linear right circular cylinder and nonlinear hourglass six WEC arrays with a 60° phase shift between the buoys with additional offset in the second group of buoys.

As shown in Figure 22 the nonlinear array of hourglass buoys delivers more power to the grid than the linear array of right circular cylinder buoys when operating in the same wave environment. To investigate the effect of the steepness angle, α, on the nonlinear buoy, the angle was varied in 5° increments from 55° to 70°, and the power delivered to the grid by the six-WEC array of nonlinear hourglass buoys was recorded. The variations in grid power for different α values are shown in Figure 23.

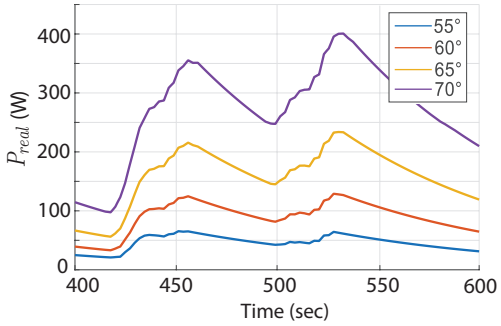

Figure 23. Power delivered to the grid by the nonlinear hourglass six WEC array for varying α values.

It was determined that the optimal value for α, the hourglass steepness angle, was 70°. The PTO and grid powers for the arrays were recorded and are shown in Table 6. Table 6 shows that the array of nonlinear hourglass WECs produces more power and delivers more power to the grid when operating in the same wave environment as a linear array of right circular cylinder WECs. Beyond the increased average power, the nonlinear hourglass array also exhibits a reduction in the variation of reactive power as shown in Figure 20. Since the energy storage is primarily needed to absorb or supply energy when the reactive power fluctuates, smaller fluctuations directly reduce the energy that the energy storage must handle.

Table 6. PTO and Grid Powers for the right circular cylinder and hourglass Six WEC Arrays in a Bretschneider Sea State.

Variable	Linear Right Circular Cylinder	NL Hourglass	Difference [%]
PTO Power	298.82 W	462.31 W	42.96
Grid Power	145.70 W	336.64 W	79.22

Arranging the WECs into a power packet network further smooths the total power delivered to the grid. By introducing phase shifts between individual WECs, the peaks and

troughs of the power from each device partially cancel, reducing both real and reactive power variability at the array level. As a result, the energy storage only needs to compensate for minor residual deviations rather than large instantaneous surges. Consequently, the required energy capacity of the energy storage can be significantly smaller, lowering system cost and complexity while maintaining stable operation and grid compatibility.

In summary, the combination of nonlinear hourglass WECs and power packet network array organization reduces fluctuations in both real and reactive power, effectively minimizing the burden on the energy storage and improving the overall wave-to-wire efficiency of the system.

7. Conclusions

This paper focused on power grid integration of wave energy converter arrays that minimized additional energy storage while maximizing power capture as well as smoothing the oscillatory power inputs into the grid. In particular, a linear right circular cylinder WEC array that implements complex conjugate control was compared and contrasted to a nonlinear WEC array that implemented an hourglass buoy shape while both are integrated into the grid utilizing phase control or relative spacing of the WEC array on the input powers to the grid. The Hamiltonians of the two systems were derived, enabling a direct comparison of real and reactive powers used by the linear and nonlinear controllers for both regular/irregular wave sea states. Note that reactive power represented the amount of stored energy required to produce real power. Once again, for the nonlinear WEC this is provided inherently by the hourglass buoy geometry, not additional energy storage system and corresponding power electronic complexity necessary, for the linear PDC3 WEC design. Our results minimized size and weight while increasing power or improving power and energy density per each individual and collective set of arrays, for the nonlinear hourglass buoy WEC. In particular, for an equivalent volume, the nonlinear WEC array produced 42.96% more PTO power than the linear array and delivered 79.22% more power to the grid than the linear array. The nonlinear buoy's maximum reactive power usage was 52.86% less than that of the linear buoy. In addition, the steepness angle, α, was adjusted to demonstrate that even more power can be achieved for the nonlinear hourglass WEC design. This proof-of-concept study successfully demonstrated the enhanced SWaP characteristics for the nonlinear hourglass WEC design for a unique power packet network array implementation. This resulted in a lower LCOE both for feasibility and economic viability. Future work will include optimizing the angle of the nonlinear hourglass WEC and the spacing between the buoys for a particular WEC deployment site with varying sea states.

Author Contributions: Conceptualization, D.W. and R.R.; Formal analysis, D.W., R.R. and W.W.; Funding acquisition, D.W.; Methodology, D.W. and W.W.; Project administration, D.W.; Software, M.V.; Supervision, W.W.; Validation, M.V.; Writing—original draft, M.V.; Writing—review and editing, D.W., R.R. and W.W. All authors have read and agreed to the published version of the manuscript.

Funding: Sandia's Advanced Grid Modeling program is supported by the U.S. Department of Energy Office of Electricity under the guidance of Ali Ghassemian. The authors would like tovthank Ali Ghassemian, for sponsoring this research as part of our Nonlinear Controls to Improve Grid Reliability and Resilience with High Penetration of Destabilizing Constant Power Loads and Generation project.

Data Availability Statement: The datapresented in this study are available on request from the corresponding author. Data are not publicly available due to institutional restrictions and data handling policies at the national laboratory where the research was conducted.

Acknowledgments: Special thanks to both Tim Donnelly and Ray Byrne at Sandia for their technical reviews. Sandia National Laboratories is a multimission laboratory managed and operated

by National Technology and Engineering Solutions of Sandia, LLC., a wholly owned subsidiary of Honeywell International, Inc., for the U.S. Department of Energy's National Nuclear Security Administration under contract DE-NA0003525. This paper describes objective technical results and analysis. Any subjective views or opinions that might be expressed in the paper do not necessarily represent the views of the U.S. Department of Energy or the United States Government.

Conflicts of Interest: The authors declare no conflicts of interest.

Abbreviations

The following abbreviations are used in this manuscript:

α	hourglass buoy steepness angle
C3	Complex conjugate control
dc	Direct current
HG	Hourglass
LCOE	Levelized cost of energy
MET	Marine energy technology
MSD	Mass-spring-damper
NL	Nonlinear
PD	Proportional-derivative
PDC3	Proportional-derivative complex conjugate controller
PMDC	Permanent magnet direct current
PPN	Power-packet-networks
PTO	Power-take-off
RCC	Right circular cylinder
SLSE	Sequential least squares estimator
SWaP	Size, weight, and power
WAFO	Wave Analysis for Fatigue Oceanography
WEC	Wave energy converter

Appendix A. Parameter Values for Right Circular Cylinder and Hourglass WEC

The parameter values for the right circular cylinder and nonlinear WEC are shown in Table A1.

Table A1. Right circular cylinder and hourglass buoy parameters.

Type	Mass (kg)	Damping Coeff. (Ns/m)	Spring Coeff. (N/m)
right circular cylinder	268	1226	1194
hourglass	268	1700	–

References

1. Kilcher, L.; Fogarty, M.; Lawson, M. *Marine Energy in the United States: An Overview of Opportunities*; Technical Report, NREL/TP-5700-78773; National Renewable Energy Laboratory: Golden, CO, USA, 2021.
2. Wiegele, J.; Jones, C. *Marine Energy Commercialization Review: Evaluation of the Transition From Public to Private Capital*; Technical Report, NREL/TP-5700-91213; National Renewable Energy Laboratory: Golden, CO, USA, 2024.
3. Wilson, D.; Robinett, R., III; Abdelkhalik, O.; Song, J.; Bacelli, G. Multi-Resonant Feedback Control of a Single Degree-of-Freedom Wave Energy Converter. U.S. Patent 10,423,126, 24 September 2019.
4. Jacobson, P.T.; Hagerman, G.; Scott, G. *Mapping and Assessment of the United States Ocean Wave Energy Resource*; Technical Report; Electric Power Research Institute: Palo Alto, CA, USA, 2011.
5. Abdelkhalik, O.; Darani, S. Optimization of nonlinear wave energy converters. *Ocean Eng.* **2018**, *162*, 187–195. [CrossRef]
6. Wilson, D.; Robinett, R., III; Weaver, W.; Glover, S. Wave Energy Converter Buoy with Variable Geometry. U.S. Patent 11,536,243, 27 December 2022.

7. Veurink, M.G.; Weaver, W.W.; Robinett, R.D., III; Wilson, D.G.; Matthews, R.C. WEC Array Optimization with Multi-Resonance and Phase Control of Electrical Power Take-Off. *IFAC-PapersOnLine* **2022**, *55*, 1–6. [CrossRef]
8. Ahamed, R.; McKee, K.; Howard, I. Advancements of wave energy converters based on power take off (PTO) systems: A review. *Ocean Eng.* **2020**, *204*, 107248. [CrossRef]
9. Weaver, W.W.; Wilson, D.G.; Hagmuller, A.; Ginsburg, M.; Bacelli, G.; Robinett, R.D.; Coe, R.; Gunawan, B. Super Capacitor Energy Storage System Design for Wave Energy Converter Demonstration. In Proceedings of the IEEE International Symposium on Power Electronics, Electrical Drives, Automation and Motion, Sorrento, Italy, 24–26 June 2020; pp. 564–570. [CrossRef]
10. Sun, P.; Li, Q.; He, H.; Chen, H.; Zhang, J.; Li, H.; Liu, D. Design and optimization investigation on hydraulic transmission and energy storage system for a floating-array-buoys wave energy converter. *Energy Convers. Manag.* **2021**, *235*, 113998. [CrossRef]
11. Prendergast, J.; Li, M.; Sheng, W. A study on the effects of wave spectra on wave energy conversions. *IEEE J. Ocean. Eng.* **2018**, *45*, 271–283. [CrossRef]
12. Bretschneider, C.L. *Wave Variability and Wave Spectra for Wind-Generated Gravity Waves*; Number 118; The Board: Washington, DC, USA, 1959.
13. Wilson, D.G.; Robinett, R.D., III; Bacelli, G.; Abdelkhalik, O.; Coe, R.G. Extending complex conjugate control to nonlinear wave energy converters. *J. Mar. Sci. Eng.* **2020**, *8*, 84. [CrossRef]
14. Fusco, F.; Ringwood, J.V. A Simple and Effective Real-Time Controller for Wave Energy Converters. *IEEE Trans. Sustain. Energy* **2012**, *4*, 21–30. [CrossRef]
15. Falnes, J.; Kurniawan, A. *Ocean Waves and Oscillating Systems: Linear Interactions Including Wave-Energy Extraction*; Cambridge University Press: Cambridge, UK, 2020; Volume 8.
16. Bacelli, G. *Optimal Control of Wave Energy Converters*; National University of Ireland: Maynooth, Ireland, 2014.
17. Toyoda, J.; Saitoh, H. Proposal of an open-electric-energy-network (OEEN) to realize cooperative operations of IOU and IPP. In Proceedings of the EMPD '98. 1998 International Conference on Energy Management and Power Delivery (Cat. No.98EX137), Singapore, 5 March 1998; Volume 1, pp. 218–222. [CrossRef]
18. Chen, M.; Poor, H.V. High-Frequency Power Electronics at the Grid Edge: A Bottom-Up Approach Toward the Smart Grid. *IEEE Electrif. Mag.* **2020**, *8*, 6–17. [CrossRef]
19. Schlichting, A.; Eisenbeiser, K. *Multifunctional Power Systems for Improved Size, Weight, and Power (SWaP) in Portable Electronic Systems*; Technical Report, MTR150029; MITRE: McLean, VA, USA, 2015.
20. Coe, R.G.; Bacelli, G.; Wilson, D.G.; Abdelkhalik, O.; Korde, U.A.; Robinett, R.D., III. A comparison of control strategies for wave energy converters. *Int. J. Mar. Energy* **2017**, *20*, 45–63. [CrossRef]
21. Kurnia, R.; Ducrozet, G. NEMO: Open-source boundary element solver for computation of first- and second-order hydrodynamic loads in the frequency domain. *Comput. Phys. Commun.* **2023**, *292*, 108885. [CrossRef]
22. Bacelli, G.; Ringwood, J. Constrained control of arrays of wave energy converters. *Int. J. Mar. Energy* **2013**, *3–4*, 53–69. [CrossRef]
23. Babarit, A. Impact of long separating distances on the energy production of two interacting wave energy converters. *Ocean Eng.* **2010**, *37*, 718–729. [CrossRef]
24. Folley, M.; Whittaker, T. The adequacy of phase-averaged models for modelling wave farms. In Proceedings of the 30th International Conference on Ocean, Offshore and Arctic Engineering (OMAE2011), Rotterdam, The Netherlands, 19–24 June 2011; Number 44373, pp. 663–671.
25. Crassidis, J.L.; Junkins, J.L. *Optimal Estimation of Dynamic Systems*; Chapman and Hall/CRC: Boca Raton, FL, USA, 2004.
26. OpenCourseWare MIT. Bretschneider Spectrum Definition. 2023. Available online: https://ocw.mit.edu/courses/2-019-design-of-ocean-systems-spring-2011/ (accessed on 8 September 2022).
27. Perez, T.; Fossen, T.I. A MATLAB toolbox for parametric identification of radiation-force models of ships and offshore structures. *Model. Identif. Control* **2009**, *30*, 1. [CrossRef]
28. Station 46073 (LLNR 1199)-SOUTHEAST BERING SEA-205 NM WNW of Dutch Harbor, AK. Available online: https://www.ndbc.noaa.gov/station_page.php?station=46073 (accessed on 17 September 2022).